



CHORUS

This is the accepted manuscript made available via CHORUS. The article has been published as:

Two-dimensional lateral GaN/SiC heterostructures: First-principles studies of electronic and magnetic properties

Guo-Xiang Chen, Xiang-Guo Li, Yun-Peng Wang, James N. Fry, and Hai-Ping Cheng

Phys. Rev. B **95**, 045302 — Published 3 January 2017

DOI: [10.1103/PhysRevB.95.045302](https://doi.org/10.1103/PhysRevB.95.045302)

Two-dimensional lateral GaN/SiC heterostructures: first-principles studies of electronic and magnetic properties

Guo-Xiang Chen,^{1,2,3} Xiang-Guo Li,^{2,3} Yun-Peng Wang,^{2,3} James N. Fry,² and Hai-Ping Cheng^{2,3*}

¹College of Sciences, Xi'an Shiyou University, Xi'an, Shaanxi 710065, PR China

²Department of Physics, University of Florida, Gainesville, FL 32611, USA

³The Quantum Theory Project, University of Florida, Gainesville, FL 32611, USA

We study the electronic and magnetic structures of quasi-one-dimensional interfaces along the zigzag direction in two dimensional GaN/SiC heterostructures using first-principles calculations. Four representative heterostructures with six inequivalent interfaces are discussed in detail. Our results indicate that a bulk electric field will develop only when both interfaces feature no gap states and the total net charge at interfaces are of opposite sign. All the geometries studied exhibit an intriguing quasi-one-dimensional conductor character, of which three show finite nonzero magnetic moment. Furthermore, the magnetic moment in one of the systems can be tuned by applying an electric field along the normal direction of monolayer indicating a strong magneto electric-coupling. Our analysis shows that the magnetization at the interfaces is closely related to the density of states at the Fermi level due to the Stoner instability, and the ribbon-width-dependent magnetization for different geometries implies the existence of an in-bulk electric field.

I. INTRODUCTION

Since the discovery of graphene¹, two-dimensional (2D) semiconductor materials have attracted extensive attention due to their novel properties and potential applications in the field of modern nanotechnology²⁻⁶. These studies show that physics at thicknesses of atomic scale can endow the 2D semiconductors with fascinating electrical, thermal, and mechanical properties that differ from those of their bulk counterparts and may bring new breakthroughs in semiconductor nanomaterials science. Among these, the III-V semiconductors, especially nitrides including hexagonal boron nitride (*h*-BN), aluminum nitride (AlN), gallium nitride (GaN), etc., are of great interest due to their many applications in optoelectronics, high-temperature, and high-power devices^{7,8}. For group III-nitrides, GaN has been investigated intensively both experimentally and theoretically⁹⁻¹¹. A wide direct band gap semiconductor (3.4 eV at room temperature), GaN is an ideal material for the fabrication of efficient short-wavelength (blue and ultraviolet) light-emitting diodes (LEDs) and room-temperature laser diodes^{12,13}.

In recent years, the synthesis of quasi one-dimensional (1D) GaN nanostructures such as nanowires, nanotubes, and nanospirals has been achieved. These novel systems are of great potential for fabricating wide-spectrum LEDs and other nanoscale devices¹⁴⁻¹⁶. Freeman et al.¹⁷ have predicted that when in the form of an ultrathin film GaN and silicon carbide (SiC) sheets transform to a 2D planar graphene-like structure. Theoretical investigations have shown that GaN and SiC monolayer sheets can form 2D stable nanostructures.¹⁸ Recently, ultrathin graphitic SiC nanoflakes with thickness down to 0.5–1.5 nm have been fabricated by Lin¹⁹ via the method of mechanical exfoliation in solution. In addition, Liu et al.²⁰ have shown that planar graphene/*h*-BN heterostructures can be formed by growing graphene in lithographically patterned *h*-BN atomic layers. On the theoretical side, AlN(ZnO)/SiC interfaces have been examined recently²¹, but only two types of stoichiometric interfaces were considered, one that can be characterized as $A_aB_bA_bB_b$ (A = cation; B = anion; a refers

to type a material and b type b) and the other as $A_bB_bA_aB_a$. So far, theoretical work has mainly focused on the electronic properties of pure low-dimensional planar materials (bulk or ribbon) such as GaN, AlN, SiC, ZnO etc.^{11,22-26}. Based on experimental developments, because of the low lattice mismatch (3.4%) between the SiC and GaN, and to potentially stimulate experimental fabrication, it merits a theoretical investigation on stability and physical properties of 2D heterogeneous GaN/SiC sheets. We thus carried out a thorough study of interfaces between the two 2D materials. Understanding the electronic and magnetic properties of the 2D heterogeneous structures can provide importance guidance for future nano-electronic device designs.

In this study, we investigate six inequivalent GaN/SiC interfaces in four geometries using the density-functional theory (DFT) method²⁷. We perform a systematic analysis of the electronic and magnetic properties of each interface. We address problems such as the physical conditions under which an electric field can appear inside the bulk material, and discuss the underlying mechanism for induced magnetization at the interfaces. The relationship between the existence of the in-bulk electric field and the characteristics of the total magnetization evolving with the ribbon width of each material are also examined.

The outline of this paper is as follows. The computational methods and model are described in Section II. Section III presents the results and a discussion, which focuses on the stability and energetics of each geometry, the electronic and magnetic properties of all the inequivalent interfaces. Finally, conclusions are given in Section IV.

II. MODEL AND METHODS

Our calculations are performed based on density-functional theory (DFT)²⁷ with the generalized gradient corrected Perdew-Burke-Ernzerhof (PBE)²⁸ exchange-correlation functional. Projector-augmented plane wave (PAW)^{29,30} potentials are used to describe the ion-electron interactions, imple-

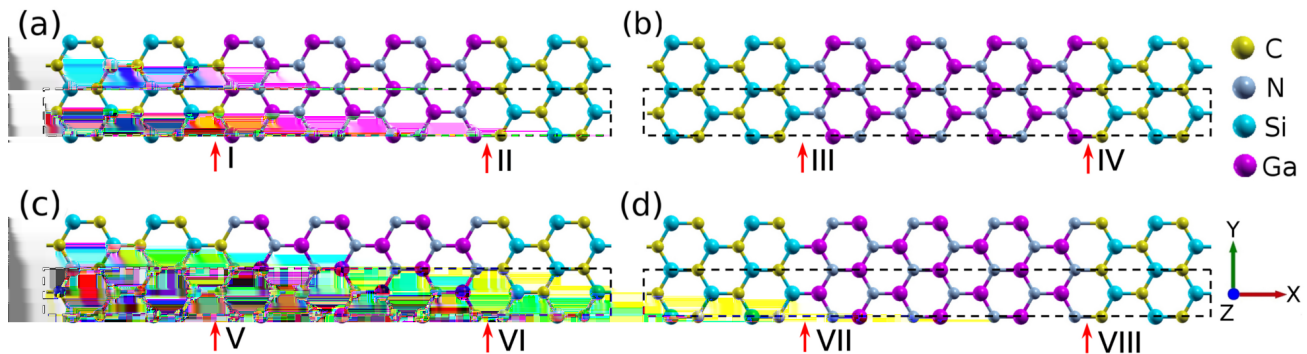


FIG. 1. (Color online) Panels (a-d) show top views of the four possible different atomic arrangements at GaN/SiC interfaces, denoted as geometries Geo 1-4. The red arrows indicate the interface positions. Each geometry has two GaN/SiC interfaces, labeled I to VIII. Dashed rectangles indicate the computational supercells of the studied systems.

mented in the Vienna *ab initio* simulation package (VASP)^{31,32}. The plane-wave cutoff is 500 eV and the threshold for self-consistency and structure relaxation are set as 10^{-5} eV and 0.01 eV/Å, respectively. A combination of $1 \times 21 \times 1$ and $1 \times 101 \times 1$ k -point samplings are applied for total energy and density of states calculations, respectively.

For calculations of the response to an external electric field, we use the effective screening medium (ESM)^{33,34} method as implemented in the QUANTUM ESPRESSO package³⁵. To apply the electric field in the direction perpendicular to the interfaces, we construct nanoribbons with structures of vacuum-SiC/GaN/SiC-vacuum and vacuum-GaN/SiC/GaN-vacuum. Edges of nanoribbons are terminated by hydrogen to remove dangling bonds. The electric field across the nanoribbons is chosen to be 0.01 V/Å.

Supercells containing two SiC/GaN interfaces along the ribbon directions are built (the y -direction in Fig.1) and the widths of ribbons are allowed to vary. In this paper we report four representative geometries (denoted as Geo 1 to Geo 4; see Fig. 1). We label the eight interfaces from I to VIII, of which the pairs II and IV and also VI and VIII are equivalent. The width of the vacuum layer has been set to be 25 Å to prevent interactions between adjacent supercells in the z -direction (Fig.1). The width of the supercell normal to the interfaces is set to be $2m$ where m is the number of zigzag chains in the ribbon, so that both the SiC and GaN nanoribbons are of width m . Because of the intermixing at interfaces I and V, the nominal widths for SiC and GaN in Geo 1 and Geo 3 are respectively $m + 1/2$ and $m - 1/2$. To make these two materials commensurate with each other, we compress the lattice of GaN along the interface direction (y -direction) since this has a lower total energy compared with that of expanding the lattice of SiC.

III. RESULTS AND DISCUSSION

A. Stability and energetics

The dynamical stability of these heterostructures is examined by calculating phonon spectra. Phonon calculations show

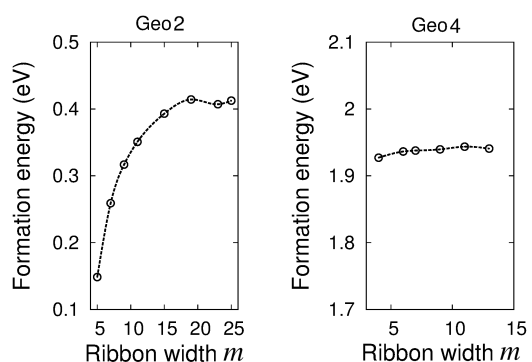


FIG. 2. (Color online) The formation energy [Eq. (1)] of heterostructures of Geo 2 and Geo 4, as a function of the ribbon width m . A spline curve is also shown as a guide to the eye.

that all the systems except for Geo 3 are dynamically stable. In Geo 3, from an imaginary phonon mode, we expect a dimerization to happen at interface V. As a result, the two C-N bonds at interface V have very different bond lengths (1.25 Å versus 2.25 Å) in the fully relaxed structure. The optimized bond lengths between the two nearest-neighbor atoms for all other interfaces are listed in Table I.

The energies of these heterostructures can be measured by using those of two-dimensional SiC and GaN materials as a

TABLE I. Interface bond lengths (between two nearest neighbors) and bonding energies for six inequivalent interface geometries.

Interface	I	II (IV)	III	V	VI (VIII)	VII
Interface geometry						
Bond length (Å)	1.90	1.94	1.69	1.25 2.25	1.44	2.37
Bonding energy (eV)	4.98	3.75	4.97	6.14	4.45	2.54

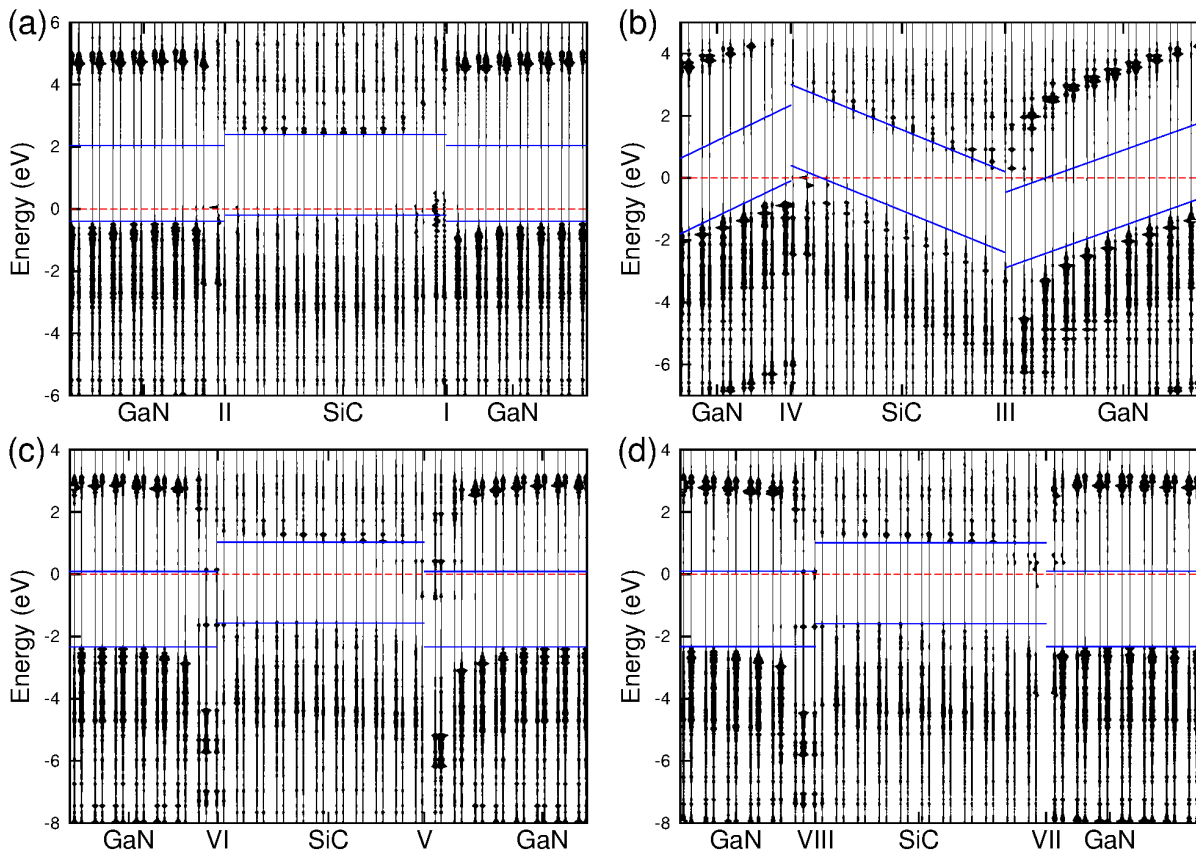


FIG. 3. (Color online) The electronic structures of two-dimensional GaN/SiC heterostructures for (a) Geo 1, (b) Geo 2, (c) Geo 3, and (d) Geo 4. The projected density of states on each atom is plotted, shifted in the x -direction by position in the heterostructure. The blue lines are used as guides to the eye of the positions of the conduction and valence bands. The Fermi energy is indicated by the red dashed lines.

reference. We define the formation energy as

$$E_{\text{formation}} = E_{\text{hetero}} - n_{\text{SiC}}E_{\text{SiC}} - n_{\text{GaN}}E_{\text{GaN}} \quad (1)$$

where E_{hetero} is the total energy of the heterostructure, the total energy of a primitive cell of GaN (SiC) is E_{GaN} (E_{SiC}), and the number of Ga-N (Si-C) pairs is n_{GaN} (n_{SiC}). Note that using Eq. (1) we can define the formation energy only for stoichiometric Geo 2 and Geo 4. The bonding energy of an interface is defined to be the energy needed to cleave the geometry along the interface without relaxation.

The formation energies of Geo 2 and Geo 4 as a function of the ribbon width m are shown in Fig. 2. The Geo 4 geometry has a formation energy nearly independent of m , which indicates that both the electronic and structural reconstructions are localized at the interfaces. The Geo 2 geometry in contrast shows an increasing formation energy as m increases, due to electrons and holes accumulated at the two interfaces (see Sec. III D). The distance between the one-dimensional electron and hole gases increases at larger m , and the Coulomb attraction between them results in an enhanced formation energy. We also note that the formation energy of Geo 4 (~ 2.0 eV) is much higher than that of Geo 2 (0.1–0.4 eV). This is a result of the anion-anion and cation-cation bonding at the interfaces of Geo 4 (for Ga-Si, the calculated

bonding energy according to Table I is 2.54 eV; for C-N this is 4.45 eV).

In this respect the interfaces in Geo 2 (Si-N: 4.97 eV and Ga-C: 3.75 eV) are very stable. The bonding energies for the interfaces (I, II, V, and VI) of the other two geometries (Geo 1 and Geo 3) shown in Table I range from 3.75 to 6.14 eV, comparable with those for the interfaces (III and IV) of Geo 2.

B. Electronic properties

The spin-resolved layer-by-layer projected density of states (DOS) of two-dimensional GaN/SiC heterostructures is shown in Fig. 3. The solid blue lines in Fig. 3 serve as a guide to the eye of the positions of maxima of the conduction and valence bands. The sawtooth shape of the blue solid lines in Fig. 3(b) indicates the presence of electric fields with opposite polarity inside GaN and SiC in Geo 2. These electric fields can be attributed to polar discontinuities, a difference between the polarizations inside GaN and inside SiC, at the interfaces^{21,36,37}. In the following we first briefly review the modern theory of polarization,^{38–40} which applies directly to the case of Geo 2, and then we analyze the different behavior in Geo 1, Geo 3, and Geo 4.

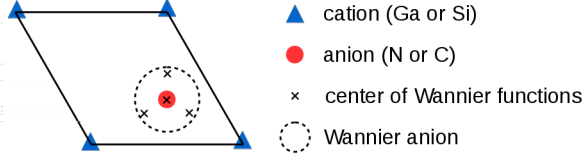


FIG. 4. (Color online) Schematic of the primitive unit cell of SiC and GaN. The positions of cations and anions are represented by triangles and filled circles. Centers of Wannier functions are represented by crosses. The Wannier anion (dashed circle) consists of one anion and its nearest neighboring Wannier functions.

The modern theory of polarization states that the contribution of an electron to the electric polarization can be represented by a point charge $-e$ located at the center of the corresponding Wannier function. These Wannier functions are constructed from all of the occupied Bloch states. Suppose that the unit cell of an insulator contains ions located at positions \mathbf{r}_α with charges \tilde{Q}_α , (the index α labels ions); and the Wannier functions of electrons are centered at \mathbf{r}_i (the index i labels electrons). The polarization in a volume Ω is then

$$\mathbf{P} = \frac{1}{\Omega} \left(\sum_{\alpha} \tilde{Q}_{\alpha} \mathbf{r}_{\alpha} - e \sum_i \mathbf{r}_i \right). \quad (2)$$

As examples, take the two 2D materials studied in this work. The volume Ω in Eq. (2) becomes the area of the unit cell; Ga and N ions have charges of $\tilde{Q} = +3e$ and $\tilde{Q} = +5e$; and Si and C ions have charges of $\tilde{Q} = +4e$ and $\tilde{Q} = +4e$. For the primitive unit cell consisting one cation (Ga or Si) and one anion (N or C), four Wannier functions can be constructed from the valence bands of bulk SiC and GaN; see Fig. 4. Each Wannier function represents a point charge of $-2e$ at its center (the factor 2 comes from spin degeneracy). One of the Wannier functions has its center located at the anion (N or C) site; the other three are located on the three anion-cation (N-Ga, or C-Si) bonds, but with a shorter distance to the anion.

One convenient approach is to combine one anion (filled circles in Fig. 4) and its four nearest neighboring Wannier functions (\times 's in Fig. 4) to form a ‘‘Wannier anion’’ (dashed circle in Fig. 4). The resulting charge of the Wannier anion at the C site is equal to that of the bare C anion ($+4e$) plus the charges of four Wannier functions ($-2e \times 4$), or $Q = +4e - 2e \times 4 = -4e$, and similarly the Wannier anion at the N site has a charge of $Q = +5e - 2e \times 4 = -3e$, while the charges of the cations are unchanged, $Q = +3e$ for Ga and $Q = +4e$ for Si. Each Wannier anion has zero dipole moment due to the threefold symmetry of the atomic structure. The expression for the polarization in Eq. (2) then becomes

$$\mathbf{P} = \frac{1}{S} \sum_{\alpha} Q_{\alpha} \mathbf{r}_{\alpha}, \quad (3)$$

where S is the area of the 2D unit cell. The positions \mathbf{r}_{α} of Wannier anions and cations are the same as those in Eq. (2). The charges Q_{α} for cations in Eq. (3) are the same as \tilde{Q}_{α} in Eq. (2), but as noted the charges Q_{α} of Wannier anions are different from the \tilde{Q}_{α} of bare anions in Eq. (2),

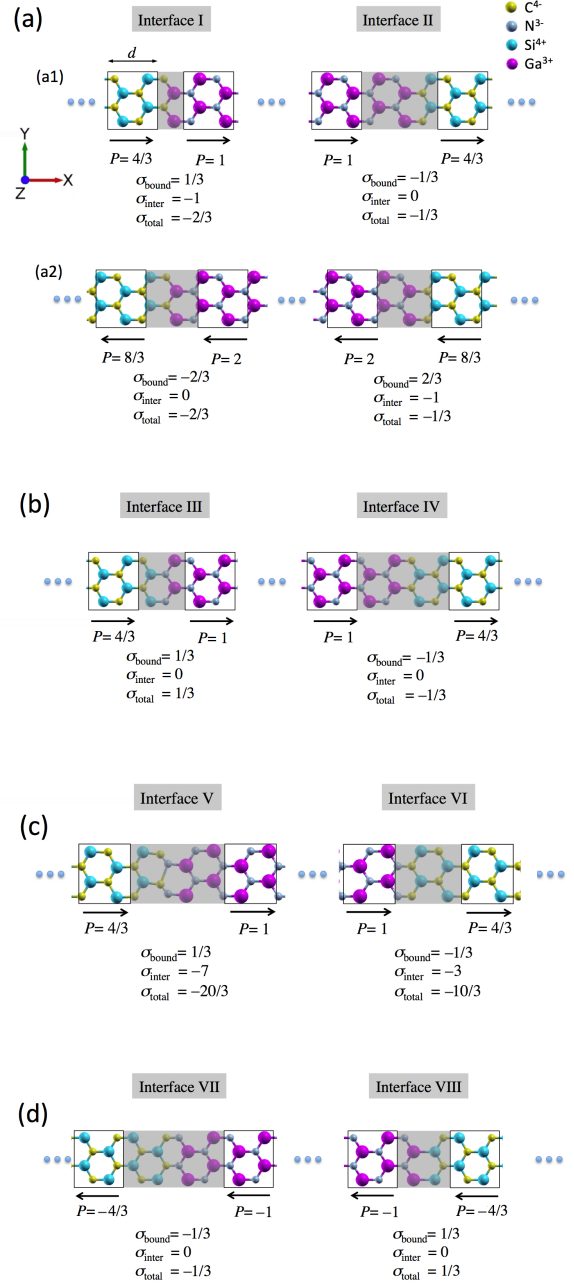


FIG. 5. (Color online) Schematic representation of the formal polarization P inside bulk GaN and SiC and the formal charge σ_{inter} at interfaces for (a) Geo 1, (b) Geo 2, (c) Geo 3, and (d) Geo 4. Interfaces are defined by shaded rectangles. For each geometry two different sets of interfaces are presented. The quantities σ and P are given in units of e/L , where L is width of the unit cell in the y -direction and e is the electron charge.

Given the electric polarization defined in Eqs. (2) and (3), electrostatics at the microscopic level obeys the same law as the classical electrostatics⁴¹; the volume density of bound charge is the divergence of the polarization, $\rho_{\text{bound}} = -\nabla \cdot \mathbf{P}$, and a polarization discontinuity corresponds to a bound interface charge. For the 1D interface between 2D SiC and GaN,

the (line) density of bound charge σ_{bound} is then equal to the discontinuity of the component of polarization normal to the interface direction,

$$\sigma_{\text{bound}} = \Delta P_x, \quad (4)$$

where we take direction normal to the 1D interface as the x -direction. Non-vanishing net charges at interfaces can then give rise to electric fields inside SiC and GaN ribbons. Hereafter the polarization and the line density of charges are expressed in unit of e/L , where L is the width of the unit cell along the direction parallel to the interface.

The analysis above can be applied directly to Geo 2. In Fig. 5(b), the unit cells of SiC and GaN are denoted by black rectangles and the interface region is highlighted by the shadow areas. The polarizations in P and in SiC and GaN are $4/3$ and 1 , respectively, so the bound charges σ_{bound} at interfaces III and IV have a density of $1/3$ and $-1/3$. Summation of the charges of Wannier anions and cations inside the interface regions gives rise to an interface charge density σ_{inter} . As shown in Fig. 5(b), both of the interfaces in Geo 2 are neutrally charged, that is $\sigma_{\text{inter}} = 0$. The total charge density σ_{total} at interfaces is

$$\sigma_{\text{total}} = \sigma_{\text{bound}} + \sigma_{\text{inter}}. \quad (5)$$

According to Gauss's law, there then is an electric field pointing from the positively charged interface III to the negatively charged interface IV. This is in accordance with the layer-projected electronic structure in Fig. 3(b).

At interfaces electrons are no longer tightly bound to anions. The potential energy difference between interfaces III and IV in Geo 2 resulting from the electric field between them increases as the distance increases; beyond a critical distance, the potential energy difference can exceed the energy band gap of bulk SiC and GaN. As a result, a long-range charge transfer occurs from interface IV to interface III.

We develop a simple one-dimensional model for describing the ribbon-width dependence of the interface charge density of Geo 2. The two interfaces IV and III are approximately treated as one-dimensional charged wires. The electrostatic potential generated by a one-dimensional charged wire with a uniform line charge density σ is,

$$V(r) = \frac{\sigma}{2\pi\epsilon} \ln \frac{r_0}{r}, \quad (6)$$

where r is the distance from the charged wire and r_0 is an arbitrary constant at which the potential is equal to zero, $V(r_0) = 0$. The dielectric constant is ϵ .

Suppose that the two interfaces in Geo 2, located at $x = 0$ and $x = m$ (m is the width for each ribbon and is equal to the number of zigzag chains), have charge densities of $-\sigma$ and $+\sigma$. The potential generated by these two interfaces along the x -direction is

$$V(x) = -\frac{\sigma}{2\pi\epsilon} \left[\ln \frac{x_1}{x} - \ln \frac{x_2}{m-x} \right]. \quad (7)$$

The constants x_1 and x_2 have no effect on the shape of $V(x)$. We choose $x_1 = x_2 = m/2$ and then have

$$V(x) = \frac{\sigma}{2\pi\epsilon} \ln \frac{x}{m-x}. \quad (8)$$

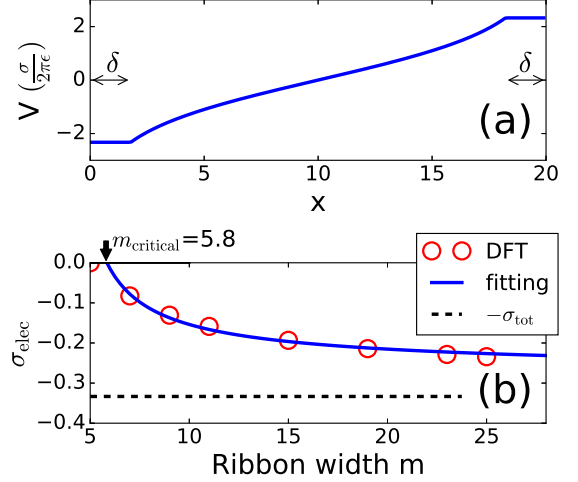


FIG. 6. (Color online) (a) The potential generated by two one-dimensional wires with charge densities $+\sigma$ and $-\sigma$ and width δ located at $x = 0$ and $x = m$. The parameters are $m = 20$ and $\delta = 1.78$. (b) The charge density from charge transfer between interfaces σ_{elec} as a function of the distance between the two interfaces. Symbols are calculated results and the curve is fitted using Eq. (11). The fitted value is $\delta = 1.78$.

The potential in Eq. (8) is divergent at $x = 0$ and at $x = m$. In order to remove the divergence, we assume that the charge density at interfaces has a finite width δ and that the potential is a constant within this width. (The units of δ are the same as the ribbon width m , that is a number of zigzag chains.) The resulting potential $V(x)$ is

$$V(x) = \begin{cases} \frac{\sigma}{2\pi\epsilon} \ln \frac{\delta}{m-\delta}, & 0 \leq x < \delta \\ \frac{\sigma}{2\pi\epsilon} \ln \frac{x}{m-x}, & \delta \leq x \leq m-\delta \\ -\frac{\sigma}{2\pi\epsilon} \ln \frac{\delta}{m-\delta}, & m-\delta < x \leq m \end{cases} \quad (9)$$

The function $V(x)$ with parameters $m = 20$ and $\delta = 1.78$ is plotted in Fig. 6(a).

The potential difference between the two interfaces is

$$\Delta V(m) = \frac{\sigma}{\pi\epsilon} \ln \frac{m-\delta}{\delta}, \quad (10)$$

which is a monotonic function of the ribbon width m . At small m ($m - \delta \approx \delta$) the potential difference is smaller than the band gap of SiC and GaN, and the interface charge density remains σ_{total} as shown in Fig. 5(b). Beyond a critical ribbon width m_{critical} , a charge transfer occurs to compensate σ_{total} ; otherwise the potential difference will exceed the gap energy E_g/e ($E_g = 2.2$ eV is equal to the smaller of the band gaps of SiC and GaN). The critical width according to our data is between $m = 5$ and $m = 7$. Above the critical width, the charge density σ at interfaces becomes the sum of σ_{total} and a compensation charge density σ_{elec} that leads to a potential difference equal to E_g/e . After substituting $\Delta V = E_g/e$ and $\sigma = \sigma_{\text{total}} + \sigma_{\text{elec}}$

in Eq. (10), we obtained σ_{elec} as a function of m ,

$$\sigma_{\text{elec}}(m) = \pi \frac{E_g \epsilon}{e} \frac{1}{\ln(m - \delta) - \ln \delta} - \sigma_{\text{total}}. \quad (11)$$

There are two unknown quantities, the width of interface charge density δ and the effective dielectric constant ϵ . A fit to our data, as shown in Fig. 6(b), gives $\epsilon = 2.31\epsilon_0$ and $\delta = 1.78$. The critical width m_{critical} is equal to 5.8.

Next we turn to Geo 1. Adopting the same analysis as for Geo 2, the polarization in bulk SiC and GaN, and the bound charge and interface charge density in Geo 1 are shown in Fig. 5(a1) and (a2) for two different choices for the bulk unit cells and interface regions. While the bound charge and the interface charge densities are different in Fig. 5(a1) and (a2), the total charge density σ_{total} is unchanged. Both of the two regions have negative total charge densities σ_{total} . Fig. 3(a) shows that the Fermi energy approaches the top of the valence band and leaves those electronic states near the interfaces partially occupied. The partial occupation of electronic states near the interface regions neutralizes the negative total charge density of Geo 1, and thus eliminates the in-ribbon electric fields.

Now we turn to Geo 3 and Geo 4. Fig. 5 indicates that Geo 3 is similar to Geo 1 in the sense that the total charges σ_{total} at interfaces have the same sign, while Geo 4 and Geo 2 seem to fall into the other category with opposite total charges at interfaces. But, as shown by their projected density of states in Fig. 3(c,d), neither does the Fermi energy of Geo 3 approach the valence or conduction bands, nor does Geo 4 show any in-ribbon electric field. In fact, Geo 3 and Geo 4 are different from Geo 1 and Geo 2 because of the presence of gap states. The projected density of states (PDOS) of Geo 4 shows the existence of some spatially localized states at interfaces. These states are located inside the energy gap of one of the materials, for instance at the interface VII the localized states near the Fermi energy is located inside the energy gap of SiC. These gap states only emerge at interfaces in Geo 3 and Geo 4, implying that they are coming from cation-cation (Ga-Si) or anion-anion (C-N) bonds. Partial occupation of these gap states compensates the total charge densities at the interface, and hence eliminate the electric field inside SiC and GaN ribbons.

C. Electric field response

To study the effects of in-sheet electric field in the directions perpendicular to interfaces, we perform ESM calculations on GaN/SiC/GaN and SiC/GaN/SiC nanoribbons of the same width. We show in Fig. 7 changes in charge density $\Delta\rho$ with and without the field. For reference, we also include simple SiC and GaN nanoribbons. The amplitude of oscillation in $\Delta\rho$ is almost uniform across the GaN nanoribbon [the upper panel of Fig. 7(a)], indicating that its edge states are inert to electric fields. In contrast, the amplitude of $\Delta\rho$ for the SiC nanoribbon [the upper panel of Fig. 7(b)] is large at the edges but reduced significantly in the interior, implying that

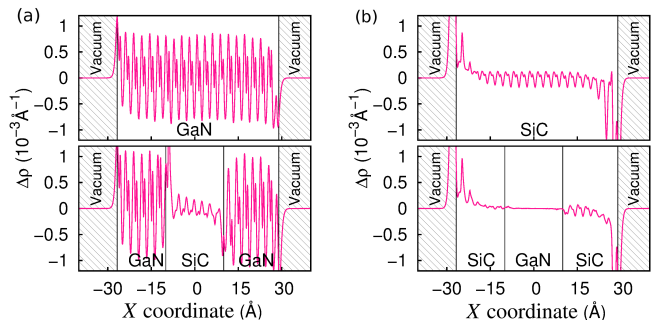


FIG. 7. (Color online) Changes of charge density in (a) GaN and GaN/SiC/GaN nanoribbons, and (b) SiC and SiC/GaN/SiC nanoribbons induced by an external electric field of 0.01 V/\AA .

the applied electric field is strongly screened by the metallic states on the zigzag edges of SiC nanoribbons. For the GaN/SiC/GaN nanoribbons, the amplitude of $\Delta\rho$ within SiC is also heavily reduced with respect to that within GaN [the bottom panel of Fig. 7(a)], which indicates that the electric field inside SiC is strongly screened by the GaN/SiC interfaces. Since the amplitude of $\Delta\rho$ inside SiC of the GaN/SiC/GaN nanoribbon [the bottom panel of Fig. 7(a)] is comparable to that in the SiC nanoribbon [the upper panel of Fig. 7(b)], the GaN/SiC interfaces show a screening capability similar to that of the zigzag edges of SiC. For the SiC/GaN/SiC nanoribbons [the bottom panel of Fig. 7(b)] the amplitude of $\Delta\rho$ inside GaN almost vanishes, because the electric field is doubly screened by the zigzag edges of SiC and by the GaN/SiC interfaces.

D. Magnetic properties and magneto-electric coupling

Our spin-resolved analysis shows a spin splitting in geometries Geo 1, Geo 2, and Geo 4. The presence of spin splitting

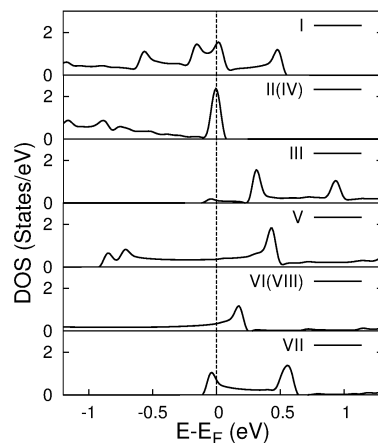


FIG. 8. (Color online) Projected density of states at each interface of Geo 1 to Geo 4 for $m = 11$ for the paramagnetic state. The smearing parameter is 0.05 eV .

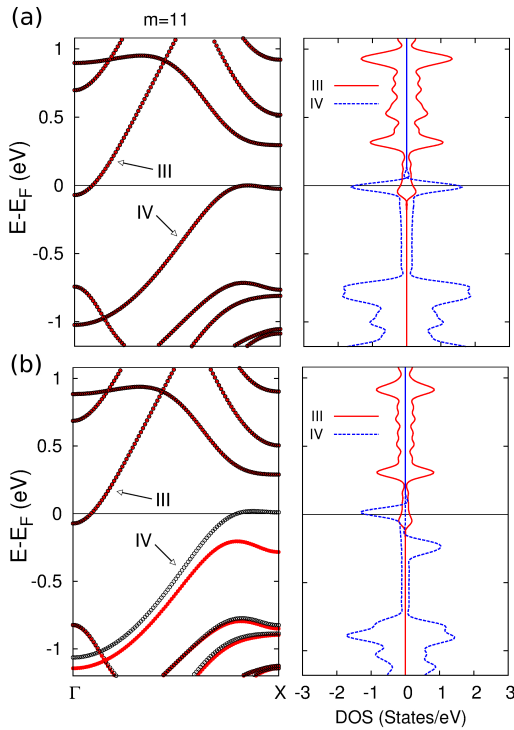


FIG. 9. (Color online) The band structure and the corresponding PDOS of each interface in GeO 2 for $m = 11$ in (a) spin-unpolarized and (b) spin-polarized states. Red and black colors in the band structure (left panel) correspond to spin-up and spin-down components, respectively. The smearing parameter in the PDOS (right panel) is $\sigma = 0.05$ eV.

in a similar system, AlN/SiC, was observed in Ref. 21, where it was explained as the result of the Stoner instability^{42,43}. The Stoner criterion^{42,43} states that a spin splitting happens at high enough DOS. To clearly observe why the spin splitting occurs at certain interfaces, we perform a spin-unpolarized calculation and project the DOS onto all interfaces, as shown in Fig. 8. Peaks in the DOS correspond to band edges. (A Gaussian smearing of 0.05 eV is used for calculating the DOS, since interfaces, as one-dimensional systems, have a divergent DOS at band edges.) We observe that there are band edges located almost at the Fermi energy for interfaces I, II (IV), and VII, leading to the spin splitting, while for the other three interfaces band edges are away from the Fermi energy, thus they are nonmagnetic.

The case of GeO 2 with width $m = 11$ is detailed in Fig. 9, which shows one spin-unpolarized (III) and one spin-polarized (IV) interface. There are two bands crossing the Fermi energy in the spin-unpolarized state [Fig. 9(a)]. One of the bands (denoted by III) is localized at interface III with a relatively steep dispersion; the corresponding DOS at the Fermi energy is very small [solid red curve in the right panel of Fig. 9(a)]. This band has its root in the conduction band of GaN. The other band (denoted by IV) is localized at interface IV and is responsible for the DOS peak at the Fermi energy (dashed blue curve), since its dispersion around the X -point is

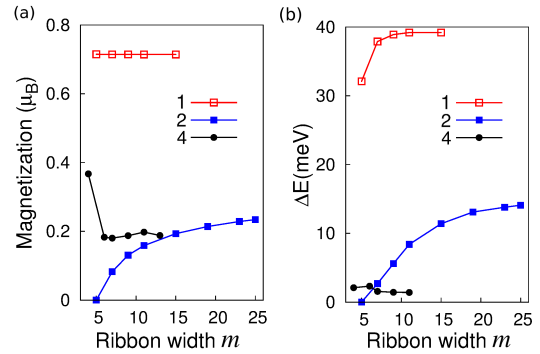


FIG. 10. (Color online) (a) The magnetization and (b) energy difference between paramagnetic and magnetic states as a function of the ribbon width m for geometries Geo 1, Geo 2, and Geo 4.

relatively flat. For the spin-polarized state the band localized at interface III remains spin-degenerate. The band localized at interface IV becomes spin-split by about 0.2 eV, and only one spin channel crosses the Fermi energy. This explains why interface IV is magnetic, and III nonmagnetic. The bands crossing the Fermi level also show a metallic character, which is verified by examining response to applied electric fields. The same arguments apply to all other interfaces. Later, we will discuss an important implication of the spin polarized charge transfer.

Stoner instability that leads to spin splitting can be measured by the total energy difference ΔE between spin-unpolarized states and polarized states. The total magnetization and the values of ΔE as a function of ribbon width m are plotted in Fig. 10. Data for Geo 3 are not shown, since both of its interfaces are spin unpolarized. The magnetization and ΔE of Geo 1 and Geo 4 converge rapidly as a function of the ribbon width m , indicating that the corresponding interface states are quite localized and the coupling between the two interfaces is negligible. The magnetization of Geo 1 is large and the spin-polarized state is quite stable. The energy difference ΔE for Geo 4 is quite small, about 1 meV per supercell, which makes the spin-polarized state stable only at very low temperature. The weak stability is related to the relatively low DOS at interface VII; the edges of bands localized at interface VII are slightly off the Fermi energy, by about 0.05 eV (see the bottom panel of Fig. 8).

The system GeO 2 shows a more interesting behavior: both its magnetization and ΔE exhibit a slow saturation with ribbon width m . In particular, when the ribbon width is small ($m \lesssim 5$), no spin-polarized phase exists. This behavior is primarily attributed to the in-bulk electric field, as discussed in Sec. III B. The polarization discontinuity at the interfaces gives rise to a macroscopic sawtooth-like potential, as shown in Fig. 3(b). When the thickness is small, the valence band maximum (VBM) at interface IV is lower in energy than the conduction band minimum (CBM) at interface III. A small band gap still exists and no DOS at Fermi level resulting in a nonmagnetic state. As the thickness increases, the VBM at interface IV eventually becomes higher in energy than the

CBM at interface III, and a charge transfer becomes favorable in energy. As indicated by the band structure plot in Fig. 9, the charge transferred from interface IV is mainly from spin-down electrons, leading to a fully spin-polarized interface. Thus the shape of the magnetization curve of Geo 2 is also the behavior of the amount of charge transfer between the two interfaces. The electron transfer increases with ribbon width, but these charges also neutralize the net charge at the interface and reduce the in-bulk electric field. As a result, the slope of the magnetization (charge transfer) curve decreases with ribbon width.

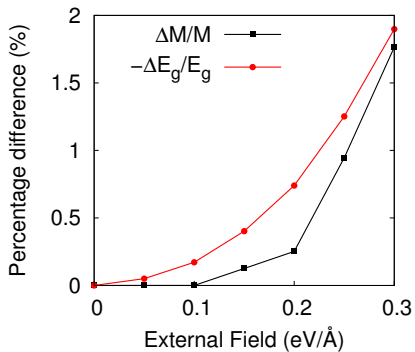


FIG. 11. (Color online) The enhancement in the magnetization and the reduction of the energy gap

Among all geometries and interfaces, interface IV in Geo 2 is unique because 1) in Geo 2 there are bond charges on the two interfaces of opposite sign, which originates an intrinsic internal electric field, 2) although cannot completely screen the field, this field drives charge hole separation across the ribbons, and 3) the holes at interface IV are fully spin-polarized. According to , the magnitude of the hole density σ_{charge} increases when the band gap E_g decreases. This relation suggests the fascinating possibility for tuning magnetic moment using electric field. According to our calculations, the energy gap of the GaN monolayer is reduced when applying an electric field perpendicular to the system. We thus further investigated the electric-field dependence of magnetization. Our results are shown in Fig. 11 with a ribbon width of $m = 11$. Under a perpendicular electric field of 0.3 V/\AA the band gap of GaN is reduced by 2%, while the magnetization at interface IV is enhanced by the same percentage. Our calculations revealed the magnetoelectric coupling in this system. The electrical manipulation of magnetization has great potential of applications in ultra-low power consumption and nonvolatile magnetoelectric memories. The mechanism for magnetoelectric coupling in this

system is different from that of single-phase materials⁴⁴, or ferromagnetic/ferroelectric composite systems^{45,46}; but is similar to the SrRuO₃/SrTiO₃ interfaces reported in Ref. 47.

IV. CONCLUSION

In conclusion, we have performed first-principles calculations on electronic structures and magnetic properties of quasi-one-dimensional interfaces in four representative GaN/SiC lateral heterostructures. Only one of the studied heterostructures shows a similar in-ribbon electric field as reported by Ref. 21, although at first sight all of the structures exhibit a polarization discontinuity. Our detailed examination establishes the conditions for the existence of an in-ribbon electric field: the absence of gap states at interfaces and an opposite sign charge accumulation at the two interfaces. Spin splitting at interfaces is detected using spin-polarized calculations, and is attributed to the appearance of band edges at the Fermi energy. Unlike in Ref. 21, where the authors reported that both left and right interfaces of an AlN ribbon are spin-polarized (the magnitude was not reported), our calculations show only interface IV in Geo 2 is (hole) spin-polarized. The ribbon-width-dependent magnetization of interfaces is closely related to the existence of the in-ribbon electric field. Specifically, the total magnetization increases gradually with ribbon width for geometries with an in-ribbon electric field, while for those without an interior electric field, the magnetization quickly converges to a constant value as the ribbon width increases. From our calculations, a model is suggested to relate the energy gap to the interface charge (Eq. 11), which lead to the important observation of a magneto-electric effect: When applying an external electric field perpendicular to the monolayer, the energy gap decreases and the interface charge increases, and ultimately the the interface magnetic moment increases significantly. An awareness of these interface properties may be of value in future electronics and spintronics applications.

ACKNOWLEDGMENTS

This work is supported by the US Department of Energy (DOE), Office of Basic Energy Sciences (BES), under Contract No. DE-FG02-02ER45995. G.-X.C. would like to acknowledge the support from the National Science Foundation of China (Grant No. 11304246) and the Science and Technology Foundation of Shaanxi Province, China (Grant No. 2014KJXX-70). The computation was done using the utilities of the National Energy Research Scientific Computing Center (NERSC).

* Email: cheng@qtp.ufl.edu; Tel: 352-392-6256

¹ K. S. Novoselov, A. K. Geim, S. Morozov, D. Jiang, Y. Zhang, S. Dubonos, I. Grigorieva, and A. Firsov, *science* **306**, 666 (2004).

² C. Xia, Y. Peng, S. Wei, and Y. Jia, *Acta Materialia* **61**, 7720 (2013).

³ D. Golberg, Y. Bando, Y. Huang, T. Terao, M. Mitome, C. Tang, and C. Zhi, *ACS Nano* **4**, 2979 (2010).

- ⁴ Y.-H. Lee, X.-Q. Zhang, W. Zhang, M.-T. Chang, C.-T. Lin, K.-D. Chang, Y.-C. Yu, J. T.-W. Wang, C.-S. Chang, L.-J. Li, *et al.*, *Advanced Materials* **24**, 2320 (2012).
- ⁵ R. Wei, J. Hu, T. Zhou, X. Zhou, J. Liu, and J. Li, *Acta Materialia* **66**, 163 (2014).
- ⁶ P. Tsipas, S. Kassavetis, D. Tsoutsou, E. Xenogiannopoulou, E. Golias, S. A. Giamini, C. Grazianetti, D. Chiappe, A. Molle, M. Fanciulli, and A. Dimoulas, *Applied Physics Letters* **103**, 251605 (2013).
- ⁷ F. Ponce and D. Bour, *Nature* **386**, 351 (1997).
- ⁸ H. Morko, S. Strite, G. B. Gao, M. E. Lin, B. Sverdlov, and M. Burns, *Journal of Applied Physics* **76**, 1363 (1994).
- ⁹ B. Heying, R. Averbeck, L. F. Chen, E. Haus, H. Riechert, and J. S. Speck, *Journal of Applied Physics* **88**, 1855 (2000).
- ¹⁰ G. Mula, C. Adelman, S. Moehl, J. Oullier, and B. Daudin, *Phys. Rev. B* **64**, 195406 (2001).
- ¹¹ Q. Chen, H. Hu, X. Chen, and J. Wang, *Applied Physics Letters* **98**, 053102 (2011).
- ¹² S. Nakamura, T. Mukai, and M. Senoh, *Applied Physics Letters* **64**, 1687 (1994).
- ¹³ S. Nakamura, *Science* **281**, 956 (1998).
- ¹⁴ T. Kuykendall, P. Ulrich, S. Aloni, and P. Yang, *Nature materials* **6**, 951 (2007).
- ¹⁵ J. Goldberger, R. He, Y. Zhang, S. Lee, H. Yan, H.-J. Choi, and P. Yang, *Nature* **422**, 599 (2003).
- ¹⁶ C. Y. Park, J. M. Lim, J. S. Yu, and Y. T. Lee, *Applied Physics Letters* **96**, 151909 (2010).
- ¹⁷ C. L. Freeman, F. Claeysens, N. L. Allan, and J. H. Harding, *Phys. Rev. Lett.* **96**, 066102 (2006).
- ¹⁸ H. Şahin, S. Cahangirov, M. Topsakal, E. Bekaroglu, E. Akturk, R. T. Senger, and S. Ciraci, *Phys. Rev. B* **80**, 155453 (2009).
- ¹⁹ S. S. Lin, *The Journal of Physical Chemistry C* **116**, 3951 (2012).
- ²⁰ Z. Liu, L. Ma, G. Shi, W. Zhou, Y. Gong, S. Lei, X. Yang, J. Zhang, J. Yu, K. P. Hackenberg, *et al.*, *Nature nanotechnology* **8**, 119 (2013).
- ²¹ N. C. Bristowe, M. Stengel, P. B. Littlewood, E. Artacho, and J. M. Pruneda, *Phys. Rev. B* **88**, 161411 (2013).
- ²² H. Li, J. Dai, J. Li, S. Zhang, J. Zhou, L. Zhang, W. Chu, D. Chen, H. Zhao, J. Yang, and Z. Wu, *The Journal of Physical Chemistry C* **114**, 11390 (2010).
- ²³ C.-w. Zhang, *Journal of Applied Physics* **111**, 043702 (2012).
- ²⁴ L. Sun, Y. Li, Z. Li, Q. Li, Z. Zhou, Z. Chen, J. Yang, and J. G. Hou, *The Journal of Chemical Physics* **129**, 174114 (2008).
- ²⁵ B. Xu, J. Yin, Y. D. Xia, X. G. Wan, and Z. G. Liu, *Applied Physics Letters* **96**, 143111 (2010).
- ²⁶ H. Guo, Y. Zhao, N. Lu, E. Kan, X. C. Zeng, X. Wu, and J. Yang, *The Journal of Physical Chemistry C* **116**, 11336 (2012).
- ²⁷ W. Kohn and L. J. Sham, *Phys. Rev.* **140**, A1133 (1965).
- ²⁸ J. P. Perdew, K. Burke, and M. Ernzerhof, *Phys. Rev. Lett.* **77**, 3865 (1996).
- ²⁹ P. E. Blöchl, O. Jepsen, and O. K. Andersen, *Phys. Rev. B* **49**, 16223 (1994).
- ³⁰ G. Kresse and D. Joubert, *Phys. Rev. B* **59**, 1758 (1999).
- ³¹ G. Kresse and J. Furthmüller, *Phys. Rev. B* **54**, 11169 (1996).
- ³² G. Kresse and J. Furthmüller, *Computational Materials Science* **6**, 15 (1996).
- ³³ Y.-P. Wang and H.-P. Cheng, *Phys. Rev. B* **91**, 245307 (2015).
- ³⁴ M. Otani and O. Sugino, *Phys. Rev. B* **73**, 115407 (2006).
- ³⁵ P. Giannozzi, S. Baroni, N. Bonini, M. Calandra, R. Car, C. Cavazzoni, D. Ceresoli, G. L. Chiarotti, M. Cococcioni, I. Dabo, A. D. Corso, S. de Gironcoli, S. Fabris, G. Fratesi, R. Gebauer, U. Gerstmann, C. Gougoussis, A. Kokalj, M. Lazzeri, L. Martin-Samos, N. Marzari, F. Mauri, R. Mazzarello, S. Paolini, A. Pasquarello, L. Paulatto, C. Sbraccia, S. Scandolo, G. Sclauzero, A. P. Seitsonen, A. Smogunov, P. Umari, and R. M. Wentzcovitch, *Journal of Physics: Condensed Matter* **21**, 395502 (2009).
- ³⁶ M. Gibertini, G. Pizzi, and N. Marzari, *Nat. Commun.* **5**, 5157 (2014).
- ³⁷ R. Martinez-Gordillo and M. Pruneda, *Progress in Surface Science* **90**, 444 (2015).
- ³⁸ D. Vanderbilt and R. D. King-Smith, *Phys. Rev. B* **48**, 4442 (1993).
- ³⁹ R. D. King-Smith and D. Vanderbilt, *Phys. Rev. B* **49**, 5828 (1994).
- ⁴⁰ R. Resta, *Rev. Mod. Phys.* **66**, 899 (1994).
- ⁴¹ M. Stengel and D. Vanderbilt, *Phys. Rev. B* **80**, 241103 (2009).
- ⁴² E. C. S. F. R. S, *Reports on Progress in Physics* **11**, 43 (1947).
- ⁴³ Y. Sun, J. D. Burton, and E. Y. Tsymlal, *Phys. Rev. B* **81**, 064413 (2010).
- ⁴⁴ A. Iyama and T. Kimura, *Phys. Rev. B* **87**, 180408 (2013).
- ⁴⁵ W. Eerenstein, M. Wiora, J. L. Prieto, J. F. Scott, and N. D. Mathur, *Nature Materials* **6**, 348 (2007).
- ⁴⁶ Z. Wang, Y. Zhang, Y. Wang, Y. Li, H. Luo, J. Li, and D. Viehland, *ACS Nano* **8**, 7793 (2014).
- ⁴⁷ J. M. Rondinelli, M. Stengel, and N. A. Spaldin, *Nature Nanotechnology* **3**, 46 (2008).